Electronic Supplementary Information

Multimode Opto-Magnetic Dual-Responsive Actuating Fibers and Fabrics Programmed by Direct Ink Writing

Supplementary Figures

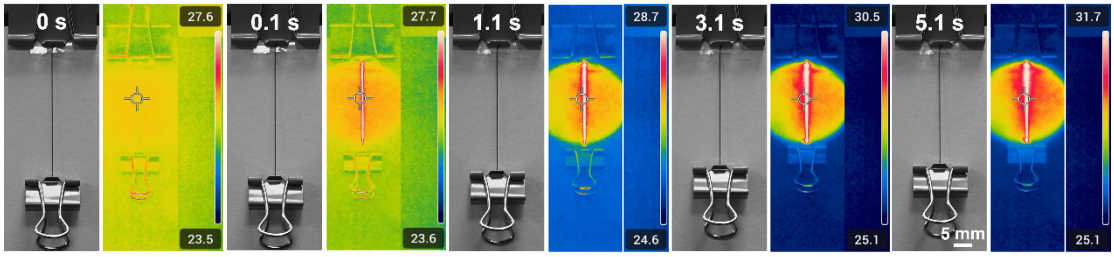

Fig. S1: Images and infrared thermal imaging of 1:4 NdFeB-LCE fibers under NIR.

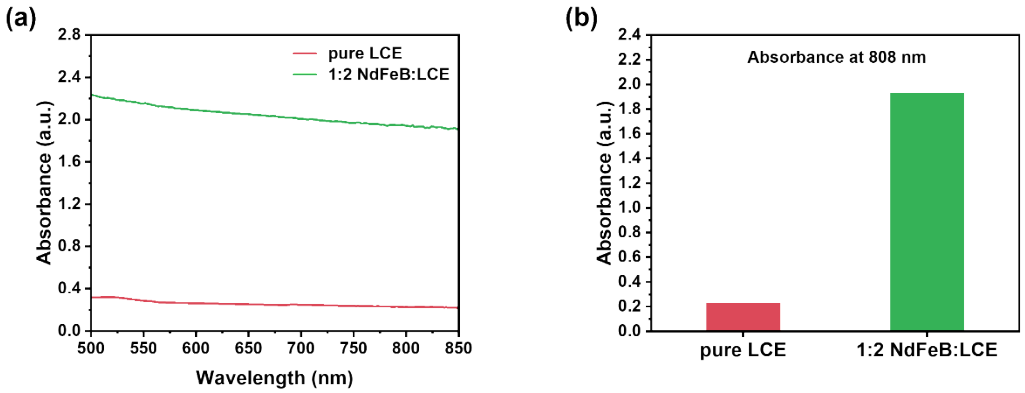

Fig. S2 (a)Absorbance in the 500~850 nm wavelength range and (b)808 nm of 1:2 NdFeB-LCE fibers.

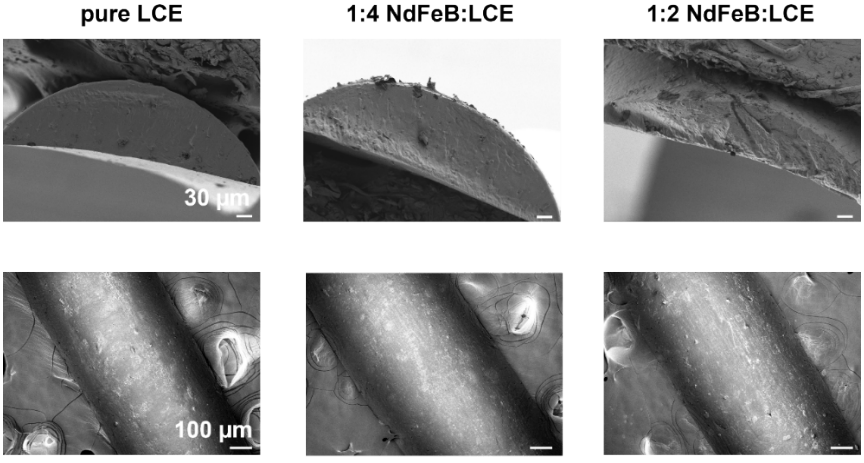

Fig. S3 SEM images showcasing the radial cross-sectional morphology (top) and surface texture (bottom) for pure LCE, 1:4 NdFeB-LCE, and 1:2 NdFeB-LCE fibers.

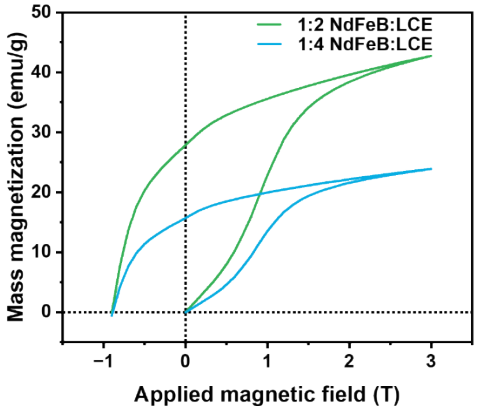

Fig. S4 Magnetization curves of NdFeB-LCE fibers.

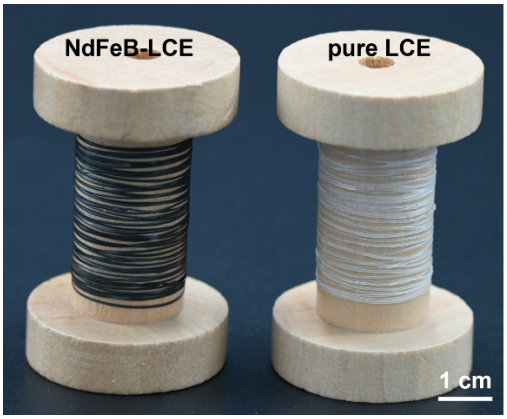

Fig. S5 Photographs of NdFeB-LCE fibers (left) and pure LCE (right).

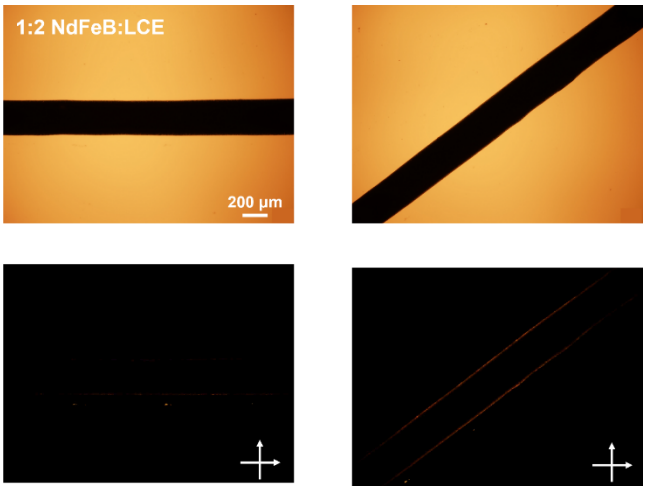

Fig. S6 Microscopic images (top) and polarized optical microscopy images (bottom) of 1:2 NdFeB-LCE fibers.

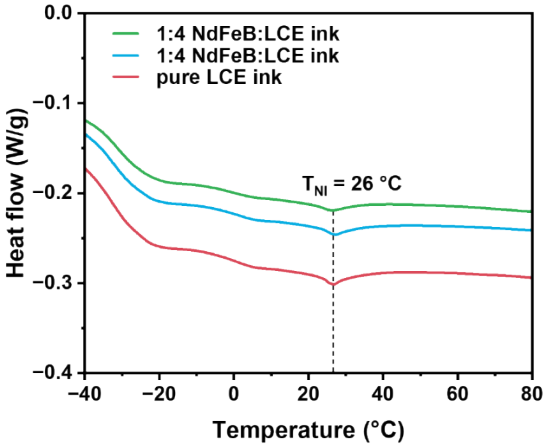

Fig. S7 Differential Scanning Calorimetry (DSC) curves of NdFeB-LCE functional oligomer ink.

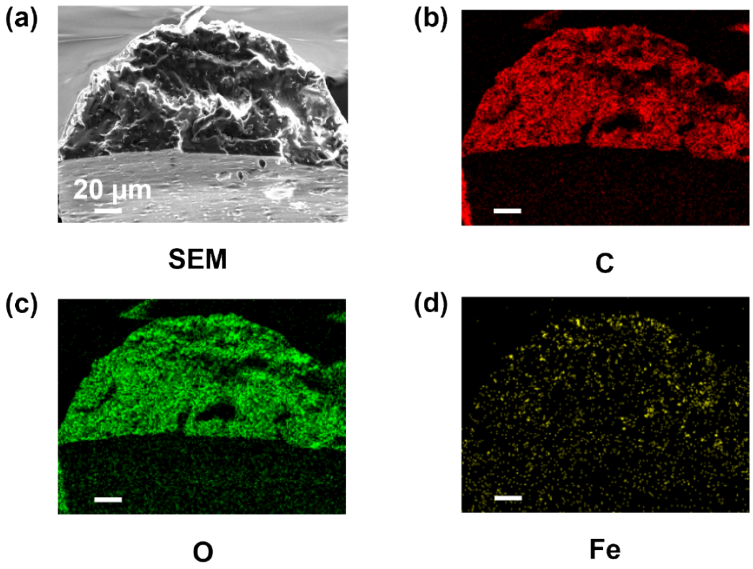

Fig. S8 (a)SEM image of the cross-section, (b)elemental distribution map for carbon, (c)elemental distribution map for oxygen, and (d)elemental distribution map for iron in NdFeB-LCE fibers

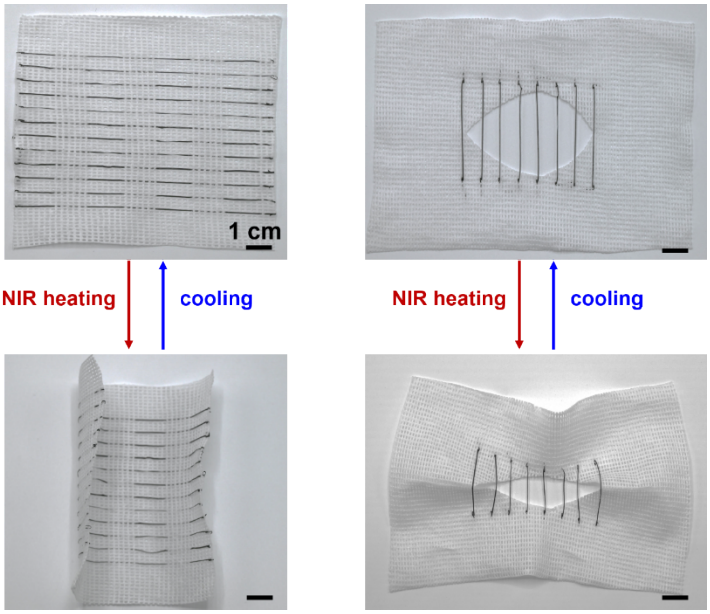

Fig. S9 NdFeB-LCE fibers are incorporated into passive textiles, resulting in the formation of smart textiles. The black fibers depicted are the NdFeB-LCE fibers.

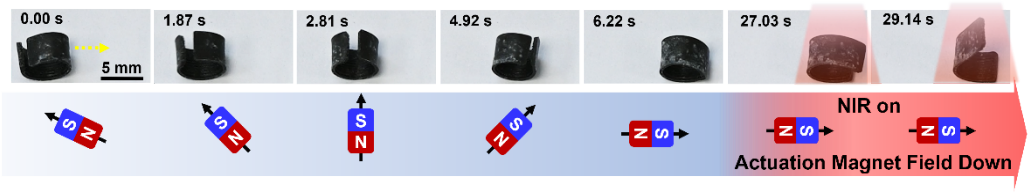

Fig. S10 Under the influence of a magnetic field, the NdFeB-LCE photomagnetic responsive fabric exhibits a rolling motion, transitioning from a "closed" to an "open" state when jointly stimulated by the magnetic field and near-infrared light.

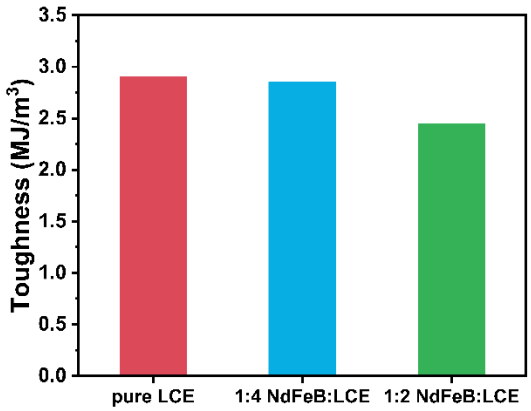

Fig. S11 Toughness of pure LCE and NdFeB-LCE fiber calculated from stress-strain curves.

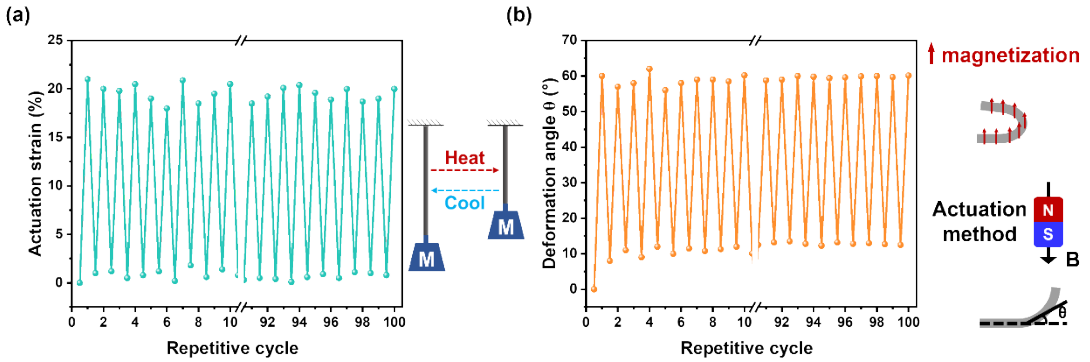

Fig. S12 (a) Cyclic actuation performance of 1:4 NdFeB-LCE fibers under a load of 1.03g heated by NIR radiation (533mW/cm^-2) for 100 cycles, with 15s of heating and 30s of cooling. (b) Cyclic actuation performance of 1:4 NdFeB-LCE fabric under an actuating magnetic field of 60mT for 100 cycles.

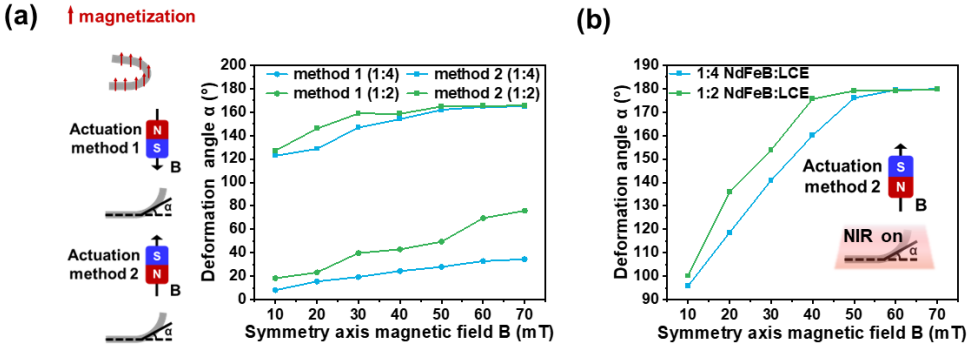

Fig. S13 (a) Response characteristics of NdFeB-LCE fabric under varied magnetic field strengths and distinct magnetic actuation modes. (b) Response characteristics of NdFeB-LCE fabric to different magnetic field intensities under NIR irradiation.

Supplementary Methods

Materials

1,4-bis-[4-(3-acryloyloxypropyloxy)benzoyloxy]-2-methylbenzene (RM257), 2,6-di-tert-butyl-4-methylphenol (BHT) and 1,3,5-triallyl-1,3,5-triazine-2,4,6(1H,3H,5H)trione (TATATO) were purchased from Bide Pharmatech (Shanghai) Co., Ltd. Ethylene glycol di(3-mercaptopropionate) (GDMP), 2,2-dimethoxy-2-phenylacetophenone (I-651) and dipropylamine (DPA) were purchased from Aladdin (Shanghai) Inc. 1,4-bis-[4-(6-acryloyloxyhexyloxy)benzoyloxy]-2-methylbenzene (RM82) was purchased from Meryer (Shanghai) Biochemical Technology Co., Ltd. NdFeB

microparticles with an average size of 5 μm (MQFP-B) were purchased from Magnequench (Korat) Co., Ltd.

Ink preparation

The thiol-terminated LCE ink was synthesized via the Michael addition reaction of thiol with acrylate. Firstly, LC monomers RM82 (0.8 g, 1.2 mmol), RM257 (0.25 g, 0.4 mmol), and the free radical inhibitor BHT (23.0 mg, 1.5 wt.%) were added into a brown glass vial. After melting at 110°C, the mixture was subjected to vortex agitation. After thorough mixing, the chain extender GDMP (0.48 g, 2 mmol) and the vinyl crosslinker TATATO (66.6 mg, 0.27 mmol) were introduced. Subsequently, the photoinitiator I-651 (23.0 mg, 1.5 wt.%) was added, followed by the catalyst DPA (5.6 mg, 0.35 wt.%). After each addition of reagents, the mixture was melted at a high temperature and subjected to vortex agitation to ensure uniform mixing. NdFeB microparticles were added to the mixture at concentrations relative to the mixture of 0 wt.%, 25 wt.%, or 50 wt.%. After melting at high temperature, the mixture underwent vortex agitation, followed by stirring with a planetary mixer for 1 minute and degassing for half a minute. The resulting mixture was kept molten to ensure good flowability and then transferred to the syringe of a dispensing machine. The mixture was left to react for 1 hour under light-free conditions, yielding pure LCE ink, 1:4 NdFeB-LCE ink, and 1:2 NdFeB-LCE ink.

DIW Fabrication of NdFeB-LCE Fibers and Fabrics

All DIW files were created using the Autodesk AutoCAD 2024 software. After exporting the files in xdf format, they were imported into the Fisnar F4403: 3-axis robotic system and then converted into lf format files. The syringe filled with ink was mounted on the Fisnar F4403: 3-axis robot. The nozzle diameter was 0.4mm (when printing fibers) or 0.25 mm (when printing fabrics). The air pump pressure was set at 700 Kpa. For active LCE fibers and fabrics, ultraviolet (UV) light curing was employed. For structurally functional but non-active LCE fibers and fabrics, after printing, they were allowed to stand at room temperature (around 26°C) for 1 minute before undergoing UV curing to reduce nematic order. All fibers and fabrics were printed onto PET plates with a uniform PVA coating. The printing nozzle was set 0.1mm above the PET substrate, and the nozzle was raised by 0.1mm for each subsequent layer. After curing, the fibers and fabrics were delaminated by rinsing with deionized water to dissolve the PVA. The NdFeB-LCE ink fibers/fabrics were then fixed in

their predetermined shapes and placed at the center of a ferromagnetic coil. Using a magnetizing machine, the fibers/fabrics were magnetized under 3T.

Characterization

The surface and cross-sectional morphology of the fibers were observed using a scanning electron microscope (ZEISS Gemini SEM 560). EDS mapping images of the NdFeB-LCE fibers were also captured. The optical properties of the fibers were characterized using a polarized optical microscope (Olympus BX53-P). The mechanical properties of the fibers were evaluated using a universal materials testing machine (Instron 5969). Differential scanning calorimetry (DSC) measurements of the ink and fibers' TNI were performed using a TA Instruments Q2500 under a nitrogen purge, with a heating/cooling rate of 10°C/min. The temperature changes in NdFeB-LCE fibers during NIR stimulation were recorded using an infrared thermal imaging camera (FLIR E96). The light absorption capability of the pure LCE fibers and NdFeB-LCE fibers was measured using a UV-Vis-NIR spectrophotometer (PerkinElmer Lambda 950). The magnetization curve and hysteresis loop of the NdFeB-LCE fibers were measured using a Physical Property Measurement System (Quantum Design PPMS-9T). Images and videos of the fibers and fabrics were captured using a digital camera (NIKON Z5).

Calculation of the Magnetic Field Strength at the Center of a Cylindrical Permanent Magnet[1]

$$B = \frac{B_r}{2}\left(\frac{D+z}{\sqrt{R^2+(D+z)^2}} - \frac{z}{\sqrt{R^2+2^2}}\right)$$

B_r: Remanence field, independent of the magnet's geometry
z: Distance from a pole face on the symmetrical axis
D: Thickness (or height) of the cylinder
R: Semi-diameter (radius) of the cylinder
The unit of length can be selected arbitrarily, as long as it is the same for all lengths.

References

1 J. M. Camacho and V. Sosa, *Rev. Mex. de Fis. E*, 2013, **59**, 8–17.